



Study of $B_{(s)}^0 \rightarrow K_S^0 h^+ h'^-$ decays with first observation of $B_s^0 \rightarrow K_S^0 K^\pm \pi^\mp$ and $B_s^0 \rightarrow K_S^0 \pi^+ \pi^-$

The LHCb collaboration[†]

Abstract

A search for charmless three-body decays of B^0 and B_s^0 mesons with a K_S^0 meson in the final state is performed using the pp collision data, corresponding to an integrated luminosity of 1.0 fb^{-1} , collected at a centre-of-mass energy of 7 TeV recorded by the LHCb experiment. Branching fractions of the $B_{(s)}^0 \rightarrow K_S^0 h^+ h'^-$ decay modes ($h^{(\prime)} = \pi, K$), relative to the well measured $B^0 \rightarrow K_S^0 \pi^+ \pi^-$ decay, are obtained. First observation of the decay modes $B_s^0 \rightarrow K_S^0 K^\pm \pi^\mp$ and $B_s^0 \rightarrow K_S^0 \pi^+ \pi^-$ and confirmation of the decay $B^0 \rightarrow K_S^0 K^\pm \pi^\mp$ are reported. The following relative branching fraction measurements or limits are obtained

$$\begin{aligned} \frac{\mathcal{B}(B^0 \rightarrow K_S^0 K^\pm \pi^\mp)}{\mathcal{B}(B^0 \rightarrow K_S^0 \pi^+ \pi^-)} &= 0.128 \pm 0.017 \text{ (stat.)} \pm 0.009 \text{ (syst.)}, \\ \frac{\mathcal{B}(B^0 \rightarrow K_S^0 K^+ K^-)}{\mathcal{B}(B^0 \rightarrow K_S^0 \pi^+ \pi^-)} &= 0.385 \pm 0.031 \text{ (stat.)} \pm 0.023 \text{ (syst.)}, \\ \frac{\mathcal{B}(B_s^0 \rightarrow K_S^0 \pi^+ \pi^-)}{\mathcal{B}(B^0 \rightarrow K_S^0 \pi^+ \pi^-)} &= 0.29 \pm 0.06 \text{ (stat.)} \pm 0.03 \text{ (syst.)} \pm 0.02 (f_s/f_d), \\ \frac{\mathcal{B}(B_s^0 \rightarrow K_S^0 K^\pm \pi^\mp)}{\mathcal{B}(B^0 \rightarrow K_S^0 \pi^+ \pi^-)} &= 1.48 \pm 0.12 \text{ (stat.)} \pm 0.08 \text{ (syst.)} \pm 0.12 (f_s/f_d), \\ \frac{\mathcal{B}(B_s^0 \rightarrow K_S^0 K^+ K^-)}{\mathcal{B}(B^0 \rightarrow K_S^0 \pi^+ \pi^-)} &\in [0.004; 0.068] \text{ at } 90\% \text{ CL}. \end{aligned}$$

Submitted to JHEP

© CERN on behalf of the LHCb collaboration, license CC-BY-3.0.

[†]Authors are listed on the following pages.

LHCb collaboration

R. Aaij⁴⁰, B. Adeva³⁶, M. Adinolfi⁴⁵, C. Adrover⁶, A. Affolder⁵¹, Z. Ajaltouni⁵, J. Albrecht⁹, F. Alessio³⁷, M. Alexander⁵⁰, S. Ali⁴⁰, G. Alkhazov²⁹, P. Alvarez Cartelle³⁶, A.A. Alves Jr^{24,37}, S. Amato², S. Amerio²¹, Y. Amhis⁷, L. Anderlini^{17,f}, J. Anderson³⁹, R. Andreassen⁵⁶, J.E. Andrews⁵⁷, R.B. Appleby⁵³, O. Aquines Gutierrez¹⁰, F. Archilli¹⁸, A. Artamonov³⁴, M. Artuso⁵⁸, E. Aslanides⁶, G. Auriemma^{24,m}, M. Baalouch⁵, S. Bachmann¹¹, J.J. Back⁴⁷, C. Baesso⁵⁹, V. Balagura³⁰, W. Baldini¹⁶, R.J. Barlow⁵³, C. Barschel³⁷, S. Barsuk⁷, W. Barter⁴⁶, Th. Bauer⁴⁰, A. Bay³⁸, J. Beddow⁵⁰, F. Bedeschi²², I. Bediaga¹, S. Belogurov³⁰, K. Belous³⁴, I. Belyaev³⁰, E. Ben-Haim⁸, G. Bencivenni¹⁸, S. Benson⁴⁹, J. Benton⁴⁵, A. Berezhnoy³¹, R. Bernet³⁹, M.-O. Bettler⁴⁶, M. van Beuzekom⁴⁰, A. Bien¹¹, S. Bifani⁴⁴, T. Bird⁵³, A. Bizzeti^{17,h}, P.M. Bjørnstad⁵³, T. Blake³⁷, F. Blanc³⁸, J. Blouw¹¹, S. Blusk⁵⁸, V. Bocci²⁴, A. Bondar³³, N. Bondar²⁹, W. Bonivento¹⁵, S. Borghi⁵³, A. Borgia⁵⁸, T.J.V. Bowcock⁵¹, E. Bowen³⁹, C. Bozzi¹⁶, T. Brambach⁹, J. van den Brand⁴¹, J. Bressieux³⁸, D. Brett⁵³, M. Britsch¹⁰, T. Britton⁵⁸, N.H. Brook⁴⁵, H. Brown⁵¹, I. Burducea²⁸, A. Bursche³⁹, G. Busetto^{21,q}, J. Buytaert³⁷, S. Cadeddu¹⁵, O. Callot⁷, M. Calvi^{20,j}, M. Calvo Gomez^{35,n}, A. Camboni³⁵, P. Campana^{18,37}, D. Campora Perez³⁷, A. Carbone^{14,c}, G. Carboni^{23,k}, R. Cardinale^{19,i}, A. Cardini¹⁵, H. Carranza-Mejia⁴⁹, L. Carson⁵², K. Carvalho Akiba², G. Casse⁵¹, L. Castillo Garcia³⁷, M. Cattaneo³⁷, Ch. Cauet⁹, R. Cenci⁵⁷, M. Charles⁵⁴, Ph. Charpentier³⁷, P. Chen^{3,38}, N. Chiapolini³⁹, M. Chrzaszcz²⁵, K. Ciba³⁷, X. Cid Vidal³⁷, G. Ciezarek⁵², P.E.L. Clarke⁴⁹, M. Clemencic³⁷, H.V. Cliff⁴⁶, J. Closier³⁷, C. Coca²⁸, V. Coco⁴⁰, J. Cogan⁶, E. Cogneras⁵, P. Collins³⁷, A. Comerma-Montells³⁵, A. Contu^{15,37}, A. Cook⁴⁵, M. Coombes⁴⁵, S. Coquereau⁸, G. Corti³⁷, B. Couturier³⁷, G.A. Cowan⁴⁹, E. Cowie⁴⁵, D.C. Craik⁴⁷, S. Cunliffe⁵², R. Currie⁴⁹, C. D'Ambrosio³⁷, P. David⁸, P.N.Y. David⁴⁰, A. Davis⁵⁶, I. De Bonis⁴, K. De Bruyn⁴⁰, S. De Capua⁵³, M. De Cian¹¹, J.M. De Miranda¹, L. De Paula², W. De Silva⁵⁶, P. De Simone¹⁸, D. Decamp⁴, M. Deckenhoff⁹, L. Del Buono⁸, N. Déléage⁴, D. Derkach⁵⁴, O. Deschamps⁵, F. Dettori⁴¹, A. Di Canto¹¹, H. Dijkstra³⁷, M. Dogaru²⁸, S. Donleavy⁵¹, F. Dordei¹¹, A. Dosil Suárez³⁶, D. Dossett⁴⁷, A. Dovbnya⁴², F. Dupertuis³⁸, P. Durante³⁷, R. Dzhelyadin³⁴, A. Dziurda²⁵, A. Dzyuba²⁹, S. Easo⁴⁸, U. Egede⁵², V. Egorychev³⁰, S. Eidelman³³, D. van Eijk⁴⁰, S. Eisenhardt⁴⁹, U. Eitschberger⁹, R. Ekelhof⁹, L. Eklund^{50,37}, I. El Rifai⁵, Ch. Elsasser³⁹, A. Falabella^{14,e}, C. Färber¹¹, G. Fardell⁴⁹, C. Farinelli⁴⁰, S. Farry⁵¹, D. Ferguson⁴⁹, V. Fernandez Albor³⁶, F. Ferreira Rodrigues¹, M. Ferro-Luzzi³⁷, S. Filippov³², M. Fiore¹⁶, C. Fitzpatrick³⁷, M. Fontana¹⁰, F. Fontanelli^{19,i}, R. Forty³⁷, O. Francisco², M. Frank³⁷, C. Frei³⁷, M. Frosini^{17,f}, S. Furcas²⁰, E. Furfaro^{23,k}, A. Gallas Torreira³⁶, D. Galli^{14,c}, M. Gandelman², P. Gandini⁵⁸, Y. Gao³, J. Garofoli⁵⁸, P. Garosi⁵³, J. Garra Tico⁴⁶, L. Garrido³⁵, C. Gaspar³⁷, R. Gauld⁵⁴, E. Gersabeck¹¹, M. Gersabeck⁵³, T. Gershon^{47,37}, Ph. Ghez⁴, V. Gibson⁴⁶, L. Giubega²⁸, V.V. Gligorov³⁷, C. Göbel⁵⁹, D. Golubkov³⁰, A. Golutvin^{52,30,37}, A. Gomes², P. Gorbounov^{30,37}, H. Gordon³⁷, C. Gotti²⁰, M. Grabalosa Gándara⁵, R. Graciani Diaz³⁵, L.A. Granado Cardoso³⁷, E. Graugés³⁵, G. Graziani¹⁷, A. Greco²⁸, E. Greening⁵⁴, S. Gregson⁴⁶, P. Griffith⁴⁴, O. Grünberg⁶⁰, B. Gui⁵⁸, E. Gushchin³², Yu. Guz^{34,37}, T. Gys³⁷, C. Hadjivasiliou⁵⁸, G. Haefeli³⁸, C. Haen³⁷, S.C. Haines⁴⁶, S. Hall⁵², B. Hamilton⁵⁷, T. Hampson⁴⁵, S. Hansmann-Menzemer¹¹, N. Harnew⁵⁴, S.T. Harnew⁴⁵, J. Harrison⁵³, T. Hartmann⁶⁰, J. He³⁷, T. Head³⁷, V. Heijne⁴⁰, K. Hennessy⁵¹, P. Henrard⁵, J.A. Hernando Morata³⁶, E. van Herwijnen³⁷, M. Hess⁶⁰, A. Hicheur¹, E. Hicks⁵¹, D. Hill⁵⁴, M. Hoballah⁵, C. Hombach⁵³, P. Hopchev⁴, W. Hulsbergen⁴⁰, P. Hunt⁵⁴, T. Huse⁵¹, N. Hussain⁵⁴, D. Hutchcroft⁵¹,

D. Hynds⁵⁰, V. Iakovenko⁴³, M. Idzik²⁶, P. Ilten¹², R. Jacobsson³⁷, A. Jaeger¹¹, E. Jans⁴⁰,
 P. Jatón³⁸, A. Jawahery⁵⁷, F. Jing³, M. John⁵⁴, D. Johnson⁵⁴, C.R. Jones⁴⁶, C. Joram³⁷,
 B. Jost³⁷, M. Kaballo⁹, S. Kandybei⁴², W. Kanso⁶, M. Karacson³⁷, T.M. Karbach³⁷,
 I.R. Kenyon⁴⁴, T. Ketel⁴¹, A. Keune³⁸, B. Khanji²⁰, O. Kochebina⁷, I. Komarov³⁸,
 R.F. Koopman⁴¹, P. Koppenburg⁴⁰, M. Korolev³¹, A. Kozlinskiy⁴⁰, L. Kravchuk³², K. Kreplin¹¹,
 M. Krepes⁴⁷, G. Krocker¹¹, P. Krokovny³³, F. Kruse⁹, M. Kucharczyk^{20,25,j}, V. Kudryavtsev³³,
 K. Kurek²⁷, T. Kvaratskheliya^{30,37}, V.N. La Thi³⁸, D. Lacarrere³⁷, G. Lafferty⁵³, A. Lai¹⁵,
 D. Lambert⁴⁹, R.W. Lambert⁴¹, E. Lanciotti³⁷, G. Lanfranchi¹⁸, C. Langenbruch³⁷,
 T. Latham⁴⁷, C. Lazzeroni⁴⁴, R. Le Gac⁶, J. van Leerdam⁴⁰, J.-P. Lees⁴, R. Lefèvre⁵,
 A. Leflat³¹, J. Lefrançois⁷, S. Leo²², O. Leroy⁶, T. Lesiak²⁵, B. Leverington¹¹, Y. Li³,
 L. Li Gioi⁵, M. Liles⁵¹, R. Lindner³⁷, C. Linn¹¹, B. Liu³, G. Liu³⁷, S. Lohn³⁷, I. Longstaff⁵⁰,
 J.H. Lopes², N. Lopez-March³⁸, H. Lu³, D. Lucchesi^{21,q}, J. Luisier³⁸, H. Luo⁴⁹, F. Machefert⁷,
 I.V. Machikhiliyan^{4,30}, F. Maciuc²⁸, O. Maev^{29,37}, S. Malde⁵⁴, G. Manca^{15,d}, G. Mancinelli⁶,
 J. Maratas⁵, U. Marconi¹⁴, P. Marino^{22,s}, R. Märki³⁸, J. Marks¹¹, G. Martellotti²⁴, A. Martens⁸,
 A. Martín Sánchez⁷, M. Martinelli⁴⁰, D. Martinez Santos⁴¹, D. Martins Tostes², A. Martynov³¹,
 A. Massafferri¹, R. Matev³⁷, Z. Mathe³⁷, C. Matteuzzi²⁰, E. Maurice⁶, A. Mazurov^{16,32,37,e},
 J. McCarthy⁴⁴, A. McNab⁵³, R. McNulty¹², B. McSkelly⁵¹, B. Meadows^{56,54}, F. Meier⁹,
 M. Meissner¹¹, M. Merk⁴⁰, D.A. Milanese⁸, M.-N. Minard⁴, J. Molina Rodriguez⁵⁹, S. Monteil⁵,
 D. Moran⁵³, P. Morawski²⁵, A. Mordà⁶, M.J. Morello^{22,s}, R. Mountain⁵⁸, I. Mous⁴⁰,
 F. Muheim⁴⁹, K. Müller³⁹, R. Muresan²⁸, B. Muryn²⁶, B. Muster³⁸, P. Naik⁴⁵, T. Nakada³⁸,
 R. Nandakumar⁴⁸, I. Nasteva¹, M. Needham⁴⁹, S. Neubert³⁷, N. Neufeld³⁷, A.D. Nguyen³⁸,
 T.D. Nguyen³⁸, C. Nguyen-Mau^{38,o}, M. Nicol⁷, V. Niess⁵, R. Niet⁹, N. Nikitin³¹, T. Nikodem¹¹,
 A. Nomerotski⁵⁴, A. Novoselov³⁴, A. Oblakowska-Mucha²⁶, V. Obraztsov³⁴, S. Oggero⁴⁰,
 S. Ogilvy⁵⁰, O. Okhrimenko⁴³, R. Oldeman^{15,d}, M. Orlandea²⁸, J.M. Otalora Goicochea²,
 P. Owen⁵², A. Oyanguren³⁵, B.K. Pal⁵⁸, A. Palano^{13,b}, T. Palczewski²⁷, M. Palutan¹⁸,
 J. Panman³⁷, A. Papanestis⁴⁸, M. Pappagallo⁵⁰, C. Parkes⁵³, C.J. Parkinson⁵², G. Passaleva¹⁷,
 G.D. Patel⁵¹, M. Patel⁵², G.N. Patrick⁴⁸, C. Patrignani^{19,i}, C. Pavel-Nicorescu²⁸,
 A. Pazos Alvarez³⁶, A. Pellegrino⁴⁰, G. Penso^{24,l}, M. Pepe Altarelli³⁷, S. Perazzini^{14,c},
 E. Perez Trigo³⁶, A. Pérez-Calero Yzquierdo³⁵, P. Perret⁵, M. Perrin-Terrin⁶, L. Pescatore⁴⁴,
 E. Pesen⁶¹, K. Petridis⁵², A. Petrolini^{19,i}, A. Phan⁵⁸, E. Picatoste Olloqui³⁵, B. Pietrzyk⁴,
 T. Pilar⁴⁷, D. Pinci²⁴, S. Playfer⁴⁹, M. Plo Casasus³⁶, F. Polci⁸, G. Polok²⁵, A. Poluektov^{47,33},
 E. Polcarpo², A. Popov³⁴, D. Popov¹⁰, B. Popovici²⁸, C. Potterat³⁵, A. Powell⁵⁴,
 J. Prisciandaro³⁸, A. Pritchard⁵¹, C. Prouve⁷, V. Pugatch⁴³, A. Puig Navarro³⁸, G. Punzi^{22,r},
 W. Qian⁴, J.H. Rademacker⁴⁵, B. Rakotomiamanana³⁸, M.S. Rangel², I. Raniuk⁴²,
 N. Rauschmayr³⁷, G. Raven⁴¹, S. Redford⁵⁴, M.M. Reid⁴⁷, A.C. dos Reis¹, S. Ricciardi⁴⁸,
 A. Richards⁵², K. Rinnert⁵¹, V. Rives Molina³⁵, D.A. Roa Romero⁵, P. Robbe⁷, D.A. Roberts⁵⁷,
 E. Rodrigues⁵³, P. Rodriguez Perez³⁶, S. Roiser³⁷, V. Romanovsky³⁴, A. Romero Vidal³⁶,
 J. Rouvinet³⁸, T. Ruf³⁷, F. Ruffini²², H. Ruiz³⁵, P. Ruiz Valls³⁵, G. Sabatino^{24,k},
 J.J. Saborido Silva³⁶, N. Sagidova²⁹, P. Sail⁵⁰, B. Saitta^{15,d}, V. Salustino Guimaraes²,
 B. Sanmartin Sedes³⁶, M. Sannino^{19,i}, R. Santacesaria²⁴, C. Santamarina Rios³⁶,
 E. Santovetti^{23,k}, M. Sapunov⁶, A. Sarti^{18,l}, C. Satriano^{24,m}, A. Satta²³, M. Savrie^{16,e},
 D. Savrina^{30,31}, P. Schaack⁵², M. Schiller⁴¹, H. Schindler³⁷, M. Schlupp⁹, M. Schmelling¹⁰,
 B. Schmidt³⁷, O. Schneider³⁸, A. Schopper³⁷, M.-H. Schune⁷, R. Schwemmer³⁷, B. Sciascia¹⁸,
 A. Sciubba²⁴, M. Seco³⁶, A. Semennikov³⁰, K. Senderowska²⁶, I. Sepp⁵², N. Serra³⁹, J. Serrano⁶,
 P. Seyfert¹¹, M. Shapkin³⁴, I. Shapoval^{16,42}, P. Shatalov³⁰, Y. Shcheglov²⁹, T. Shears^{51,37},
 L. Shekhtman³³, O. Shevchenko⁴², V. Shevchenko³⁰, A. Shires⁹, R. Silva Coutinho⁴⁷,

M. Sirendi⁴⁶, N. Skidmore⁴⁵, T. Skwarnicki⁵⁸, N.A. Smith⁵¹, E. Smith^{54,48}, J. Smith⁴⁶, M. Smith⁵³, M.D. Sokoloff⁵⁶, F.J.P. Soler⁵⁰, F. Soomro³⁸, D. Souza⁴⁵, B. Souza De Paula², B. Spaan⁹, A. Sparkes⁴⁹, P. Spradlin⁵⁰, F. Stagni³⁷, S. Stahl¹¹, O. Steinkamp³⁹, S. Stevenson⁵⁴, S. Stoica²⁸, S. Stone⁵⁸, B. Storaci³⁹, M. Straticiuc²⁸, U. Straumann³⁹, V.K. Subbiah³⁷, L. Sun⁵⁶, S. Swientek⁹, V. Syropoulos⁴¹, M. Szczekowski²⁷, P. Szczypka^{38,37}, T. Szumlak²⁶, S. T’Jampens⁴, M. Teklishyn⁷, E. Teodorescu²⁸, F. Teubert³⁷, C. Thomas⁵⁴, E. Thomas³⁷, J. van Tilburg¹¹, V. Tisserand⁴, M. Tobin³⁸, S. Tolk⁴¹, D. Tonelli³⁷, S. Topp-Joergensen⁵⁴, N. Torr⁵⁴, E. Tournefier^{4,52}, S. Tourneur³⁸, M.T. Tran³⁸, M. Tresch³⁹, A. Tsaregorodtsev⁶, P. Tsopelas⁴⁰, N. Tuning⁴⁰, M. Ubeda Garcia³⁷, A. Ukleja²⁷, D. Urner⁵³, A. Ustyuzhanin^{52,p}, U. Uwer¹¹, V. Vagnoni¹⁴, G. Valenti¹⁴, A. Vallier⁷, M. Van Dijk⁴⁵, R. Vazquez Gomez¹⁸, P. Vazquez Regueiro³⁶, C. Vázquez Sierra³⁶, S. Vecchi¹⁶, J.J. Velthuis⁴⁵, M. Veltri^{17,g}, G. Veneziano³⁸, M. Vesterinen³⁷, B. Viaud⁷, D. Vieira², X. Vilasis-Cardona^{35,n}, A. Vollhardt³⁹, D. Volyanskyy¹⁰, D. Voong⁴⁵, A. Vorobyev²⁹, V. Vorobyev³³, C. Voß⁶⁰, H. Voss¹⁰, R. Waldi⁶⁰, C. Wallace⁴⁷, R. Wallace¹², S. Wandernoth¹¹, J. Wang⁵⁸, D.R. Ward⁴⁶, N.K. Watson⁴⁴, A.D. Webber⁵³, D. Websdale⁵², M. Whitehead⁴⁷, J. Wicht³⁷, J. Wiechczynski²⁵, D. Wiedner¹¹, L. Wiggers⁴⁰, G. Wilkinson⁵⁴, M.P. Williams^{47,48}, M. Williams⁵⁵, F.F. Wilson⁴⁸, J. Wimberley⁵⁷, J. Wishahi⁹, W. Wislicki²⁷, M. Witek²⁵, S.A. Wotton⁴⁶, S. Wright⁴⁶, S. Wu³, K. Wyllie³⁷, Y. Xie^{49,37}, Z. Xing⁵⁸, Z. Yang³, R. Young⁴⁹, X. Yuan³, O. Yushchenko³⁴, M. Zangoli¹⁴, M. Zavertyaev^{10,a}, F. Zhang³, L. Zhang⁵⁸, W.C. Zhang¹², Y. Zhang³, A. Zhelezov¹¹, A. Zhokhov³⁰, L. Zhong³, A. Zvyagin³⁷.

¹Centro Brasileiro de Pesquisas Físicas (CBPF), Rio de Janeiro, Brazil

²Universidade Federal do Rio de Janeiro (UFRJ), Rio de Janeiro, Brazil

³Center for High Energy Physics, Tsinghua University, Beijing, China

⁴LAPP, Université de Savoie, CNRS/IN2P3, Annecy-Le-Vieux, France

⁵Clermont Université, Université Blaise Pascal, CNRS/IN2P3, LPC, Clermont-Ferrand, France

⁶CPPM, Aix-Marseille Université, CNRS/IN2P3, Marseille, France

⁷LAL, Université Paris-Sud, CNRS/IN2P3, Orsay, France

⁸LPNHE, Université Pierre et Marie Curie, Université Paris Diderot, CNRS/IN2P3, Paris, France

⁹Fakultät Physik, Technische Universität Dortmund, Dortmund, Germany

¹⁰Max-Planck-Institut für Kernphysik (MPIK), Heidelberg, Germany

¹¹Physikalisches Institut, Ruprecht-Karls-Universität Heidelberg, Heidelberg, Germany

¹²School of Physics, University College Dublin, Dublin, Ireland

¹³Sezione INFN di Bari, Bari, Italy

¹⁴Sezione INFN di Bologna, Bologna, Italy

¹⁵Sezione INFN di Cagliari, Cagliari, Italy

¹⁶Sezione INFN di Ferrara, Ferrara, Italy

¹⁷Sezione INFN di Firenze, Firenze, Italy

¹⁸Laboratori Nazionali dell’INFN di Frascati, Frascati, Italy

¹⁹Sezione INFN di Genova, Genova, Italy

²⁰Sezione INFN di Milano Bicocca, Milano, Italy

²¹Sezione INFN di Padova, Padova, Italy

²²Sezione INFN di Pisa, Pisa, Italy

²³Sezione INFN di Roma Tor Vergata, Roma, Italy

²⁴Sezione INFN di Roma La Sapienza, Roma, Italy

²⁵Henryk Niewodniczanski Institute of Nuclear Physics Polish Academy of Sciences, Kraków, Poland

²⁶AGH - University of Science and Technology, Faculty of Physics and Applied Computer Science, Kraków, Poland

²⁷National Center for Nuclear Research (NCBJ), Warsaw, Poland

- ²⁸ *Horia Hulubei National Institute of Physics and Nuclear Engineering, Bucharest-Magurele, Romania*
- ²⁹ *Petersburg Nuclear Physics Institute (PNPI), Gatchina, Russia*
- ³⁰ *Institute of Theoretical and Experimental Physics (ITEP), Moscow, Russia*
- ³¹ *Institute of Nuclear Physics, Moscow State University (SINP MSU), Moscow, Russia*
- ³² *Institute for Nuclear Research of the Russian Academy of Sciences (INR RAN), Moscow, Russia*
- ³³ *Budker Institute of Nuclear Physics (SB RAS) and Novosibirsk State University, Novosibirsk, Russia*
- ³⁴ *Institute for High Energy Physics (IHEP), Protvino, Russia*
- ³⁵ *Universitat de Barcelona, Barcelona, Spain*
- ³⁶ *Universidad de Santiago de Compostela, Santiago de Compostela, Spain*
- ³⁷ *European Organization for Nuclear Research (CERN), Geneva, Switzerland*
- ³⁸ *Ecole Polytechnique Fédérale de Lausanne (EPFL), Lausanne, Switzerland*
- ³⁹ *Physik-Institut, Universität Zürich, Zürich, Switzerland*
- ⁴⁰ *Nikhef National Institute for Subatomic Physics, Amsterdam, The Netherlands*
- ⁴¹ *Nikhef National Institute for Subatomic Physics and VU University Amsterdam, Amsterdam, The Netherlands*
- ⁴² *NSC Kharkiv Institute of Physics and Technology (NSC KIPT), Kharkiv, Ukraine*
- ⁴³ *Institute for Nuclear Research of the National Academy of Sciences (KINR), Kyiv, Ukraine*
- ⁴⁴ *University of Birmingham, Birmingham, United Kingdom*
- ⁴⁵ *H.H. Wills Physics Laboratory, University of Bristol, Bristol, United Kingdom*
- ⁴⁶ *Cavendish Laboratory, University of Cambridge, Cambridge, United Kingdom*
- ⁴⁷ *Department of Physics, University of Warwick, Coventry, United Kingdom*
- ⁴⁸ *STFC Rutherford Appleton Laboratory, Didcot, United Kingdom*
- ⁴⁹ *School of Physics and Astronomy, University of Edinburgh, Edinburgh, United Kingdom*
- ⁵⁰ *School of Physics and Astronomy, University of Glasgow, Glasgow, United Kingdom*
- ⁵¹ *Oliver Lodge Laboratory, University of Liverpool, Liverpool, United Kingdom*
- ⁵² *Imperial College London, London, United Kingdom*
- ⁵³ *School of Physics and Astronomy, University of Manchester, Manchester, United Kingdom*
- ⁵⁴ *Department of Physics, University of Oxford, Oxford, United Kingdom*
- ⁵⁵ *Massachusetts Institute of Technology, Cambridge, MA, United States*
- ⁵⁶ *University of Cincinnati, Cincinnati, OH, United States*
- ⁵⁷ *University of Maryland, College Park, MD, United States*
- ⁵⁸ *Syracuse University, Syracuse, NY, United States*
- ⁵⁹ *Pontifícia Universidade Católica do Rio de Janeiro (PUC-Rio), Rio de Janeiro, Brazil, associated to ²*
- ⁶⁰ *Institut für Physik, Universität Rostock, Rostock, Germany, associated to ¹¹*
- ⁶¹ *Celal Bayar University, Manisa, Turkey, associated to ³⁷*

^a *P.N. Lebedev Physical Institute, Russian Academy of Science (LPI RAS), Moscow, Russia*

^b *Università di Bari, Bari, Italy*

^c *Università di Bologna, Bologna, Italy*

^d *Università di Cagliari, Cagliari, Italy*

^e *Università di Ferrara, Ferrara, Italy*

^f *Università di Firenze, Firenze, Italy*

^g *Università di Urbino, Urbino, Italy*

^h *Università di Modena e Reggio Emilia, Modena, Italy*

ⁱ *Università di Genova, Genova, Italy*

^j *Università di Milano Bicocca, Milano, Italy*

^k *Università di Roma Tor Vergata, Roma, Italy*

^l *Università di Roma La Sapienza, Roma, Italy*

^m *Università della Basilicata, Potenza, Italy*

ⁿ *LIFAEELS, La Salle, Universitat Ramon Llull, Barcelona, Spain*

^o *Hanoi University of Science, Hanoi, Viet Nam*

^p *Institute of Physics and Technology, Moscow, Russia*

^q*Università di Padova, Padova, Italy*

^r*Università di Pisa, Pisa, Italy*

^s*Scuola Normale Superiore, Pisa, Italy*

1 Introduction

The study of the charmless three-body decays of neutral B mesons to final states including a K_s^0 meson, namely $B_{(s)}^0 \rightarrow K_s^0 \pi^+ \pi^-$, $B_{(s)}^0 \rightarrow K_s^0 K^\pm \pi^\mp$ and $B_{(s)}^0 \rightarrow K_s^0 K^+ K^-$, has a number of theoretical applications.¹ The decays $B^0 \rightarrow K_s^0 \pi^+ \pi^-$ and $B^0 \rightarrow K_s^0 K^+ K^-$ are dominated by $b \rightarrow q \bar{q} s$ ($q = u, d, s$) loop transitions. Mixing-induced CP asymmetries in such decays are predicted to be approximately equal to those in $b \rightarrow c \bar{c} s$ transitions, *e.g.* $B^0 \rightarrow J/\psi K_s^0$, by the Cabibbo-Kobayashi-Maskawa mechanism [1, 2]. However, the loop diagrams that dominate the charmless decays can have contributions from new particles in several extensions of the Standard Model, which could introduce additional weak phases [3–6]. A time-dependent analysis of the three-body Dalitz plot allows measurements of the mixing-induced CP -violating phase [7–10]. The current experimental measurements of $b \rightarrow q \bar{q} s$ decays [11] show fair agreement with the results from $b \rightarrow c \bar{c} s$ decays (measuring the weak phase β) for each of the scrutinised CP eigenstates. There is, however, a global trend towards lower values than the weak phase measured from $b \rightarrow c \bar{c} s$ decays. The interpretation of this deviation is made complicated by QCD corrections, which depend on the final state [12] and are difficult to handle. An analogous extraction of the mixing-induced CP -violating phase in the B_s^0 system will, with a sufficiently large dataset, also be possible with the $B_s^0 \rightarrow K_s^0 K^\pm \pi^\mp$ decay, which can be compared with that from, *e.g.* $B_s^0 \rightarrow J/\psi \phi$.

Much recent theoretical and experimental activity has focused on the determination of the CKM angle γ from $B \rightarrow K \pi \pi$ decays, using and refining the methods proposed in Refs. [13, 14]. The recent experimental results from BaBar [15] demonstrate the feasibility of the method, albeit with large statistical uncertainties. The decay $B_s^0 \rightarrow K_s^0 \pi^+ \pi^-$ is of particular interest for this effort. Indeed, the ratio of the amplitudes of the isospin-related mode $B_s^0 \rightarrow K^- \pi^+ \pi^0$ and its charge conjugate exhibits a direct dependence on the mixing-induced CP -violating phase, which would be interpreted in the Standard Model as $(\beta_s + \gamma)$. Unlike the equivalent B^0 decays, the B_s^0 decays are dominated by tree amplitudes and the contributions from electroweak penguin diagrams are expected to be negligible, yielding a theoretically clean extraction of γ [16] provided that the strong phase can be determined from other measurements. The shared intermediate states between $B_s^0 \rightarrow K^- \pi^+ \pi^0$ and $B_s^0 \rightarrow K_s^0 \pi^+ \pi^-$ (specifically $K^{*-} \pi^+$) offer that possibility, requiring an analysis of the $B_s^0 \rightarrow K_s^0 \pi^+ \pi^-$ Dalitz plot.

At LHCb, the first step towards this physics programme is to establish the signals of all the decay modes. In particular, the decay modes $B_s^0 \rightarrow K_s^0 h^+ h'^-$ ($h^{(\prime)} = \pi, K$) are all unobserved and the observation of $B^0 \rightarrow K_s^0 K^\pm \pi^\mp$ by BaBar [17] is so far unconfirmed. In this paper the results of an analysis of all six $B_{(s)}^0 \rightarrow K_s^0 h^+ h'^-$ decay modes are presented. The branching fractions of the decay modes relative to that of $B^0 \rightarrow K_s^0 \pi^+ \pi^-$ are measured when the significance of the signals allow it, otherwise confidence intervals are quoted. Time-integrated branching fractions are computed, implying a non-trivial comparison of the B^0 and B_s^0 decays at amplitude level [18].

¹Unless stated otherwise, charge conjugated modes are implicitly included throughout the paper.

2 Detector and dataset

The measurements described in this paper are performed with data, corresponding to an integrated luminosity of 1.0 fb^{-1} , from 7 TeV centre-of-mass pp collisions, collected with the LHCb detector during 2011. Samples of simulated events are used to estimate the efficiency of the selection requirements, to investigate possible sources of background contributions, and to model the event distributions in the likelihood fit. In the simulation, pp collisions are generated using PYTHIA 6.4 [19] with a specific LHCb configuration [20]. Decays of hadronic particles are described by EVTGEN [21], in which final state radiation is generated using PHOTOS [22]. The interaction of the generated particles with the detector and its response are implemented using the GEANT4 toolkit [23] as described in Ref. [24].

The LHCb detector [25] is a single-arm forward spectrometer covering the pseudorapidity range $2 < \eta < 5$, designed for the study of particles containing b or c quarks. The detector includes a high-precision tracking system consisting of a silicon-strip vertex detector (VELO) surrounding the pp interaction region, a large-area silicon-strip detector located upstream of a dipole magnet with a bending power of about 4 Tm, and three stations of silicon-strip detectors and straw drift tubes placed downstream. The combined tracking system provides a momentum measurement with relative uncertainty that varies from 0.4% at 5 GeV/ c to 0.6% at 100 GeV/ c , and impact parameter resolution of 20 μm for tracks with high transverse momentum. Charged hadrons are identified using two ring-imaging Cherenkov (RICH) detectors [26]. Photon, electron and hadron candidates are identified by a calorimeter system consisting of scintillating-pad and preshower detectors, an electromagnetic calorimeter and a hadronic calorimeter. Muons are identified by a system composed of alternating layers of iron and multiwire proportional chambers.

3 Trigger and event selection

The trigger [27] consists of a hardware stage, based on information from the calorimeter and muon systems, followed by a software stage, which applies a full event reconstruction. To remove events with large occupancies, a requirement is made at the hardware stage on the number of hits in the scintillating-pad detector. The hadron trigger at the hardware stage also requires that there is at least one candidate with transverse energy $E_T > 3.5 \text{ GeV}$. In the offline selection, candidates are separated into two categories based on the hardware trigger decision. The first category are triggered by particles from candidate signal decays that have an associated cluster in the calorimeters above the threshold, while the second category are triggered independently of the particles associated with the signal decay. Events that do not fall into either of these categories are not used in the subsequent analysis.

The software trigger requires a two-, three- or four-track secondary vertex with a high sum of the transverse momentum, p_T , of the tracks and significant displacement from the primary pp interaction vertices (PVs). At least one track should have $p_T > 1.7 \text{ GeV}/c$ and χ_{IP}^2 with respect to any primary interaction greater than 16, where χ_{IP}^2 is defined as the difference in χ^2 of a given PV reconstructed with and without the considered track. A

multivariate algorithm [28] is used for the identification of secondary vertices consistent with the decay of a b hadron.

The events passing the trigger requirements are then filtered in two stages. Initial requirements are applied to further reduce the size of the data sample, before a multivariate selection is implemented. In order to minimise the variation of the selection efficiency over the Dalitz plot it is necessary to place only loose requirements on the momenta of the daughter particles. As a consequence, selection requirements on topological variables such as the flight distance of the B candidate or the direction of its momentum vector are used as the main discriminants.

The K_s^0 candidates are reconstructed in the $\pi^+\pi^-$ final state. Approximately two thirds of the reconstructed K_s^0 mesons decay downstream of the VELO. Since those K_s^0 candidates decaying within the VELO, and those that have information only from the tracking stations, differ in their reconstruction and selection, they are separated into two categories labelled “Long” and “Downstream”, respectively. The pions that form the K_s^0 candidates are required to have momentum $p > 2 \text{ GeV}/c$ and χ_{IP}^2 with respect to any PV greater than 9 (4) for Long (Downstream) K_s^0 candidates. The K_s^0 candidates are then required to form a vertex with $\chi_{\text{vtx}}^2 < 12$ and to have invariant mass within $20 \text{ MeV}/c^2$ ($30 \text{ MeV}/c^2$) of the nominal K_s^0 mass [29] for Long (Downstream) candidates. The square of the separation of the K_s^0 vertex from the PV divided by the associated uncertainty (χ_{VS}^2) must be greater than 80 (50) for Long (Downstream) candidates. Downstream K_s^0 candidates are required, in addition, to have momentum $p > 6 \text{ GeV}/c$.

The B candidates are formed by combining the K_s^0 candidates with two oppositely charged tracks. Selection requirements, common to both the Long and Downstream categories, are based on the topology and kinematics of the B candidate. The charged B -meson daughters are required to have $p < 100 \text{ GeV}/c$, a momentum beyond which there is little pion/kaon discrimination. The scalar sum of the three daughters’ transverse momenta must be greater than $3 \text{ GeV}/c$, and at least two of the daughters must have $p_{\text{T}} > 0.8 \text{ GeV}/c$. The impact parameter (IP) of the B -meson daughter with the largest p_{T} is required to be greater than 0.05 mm relative to the PV associated to the B candidate. The χ^2 of the distance of closest approach of any two daughters must be less than 5. The B candidates are then required to form a vertex separated from any PV by at least 1 mm and that has $\chi_{\text{vtx}}^2 < 12$ and $\chi_{\text{VS}}^2 > 50$. The difference in χ_{vtx}^2 when adding any track must be greater than 4. The candidates must have $p_{\text{T}} > 1.5 \text{ GeV}/c$ and invariant mass within the range $4779 < m_{K_s^0 h^+ h'^-} < 5866 \text{ MeV}/c^2$. The cosine of the angle between the reconstructed momentum of the B meson and its direction of flight (pointing angle) is required to be greater than 0.9999. The candidates are further required to have a minimum χ_{IP}^2 with respect to all PVs less than 4. Finally, the separation of the K_s^0 and B vertices in the positive z direction² must be greater than 30 mm .

Multivariate discriminants based on a boosted decision tree (BDT) [30] with the AdaBoost algorithm [31] have been designed in order to complete the selection of the signal events and to further reject combinatorial backgrounds. Simulated $B_{(s)}^0 \rightarrow K_s^0 \pi^+ \pi^-$

²The z axis points along the beam line from the interaction region through the LHCb detector.

events and upper mass sidebands, $5420 < m_{K_s^0 \pi^+ \pi^-} < 5866 \text{ MeV}/c^2$, in the data are used as the signal and background training samples, respectively. The samples of events in each of the Long and Downstream K_s^0 categories are further subdivided into two equally-sized subsamples. Each subsample is then used to train an independent discriminant. In the subsequent analysis the BDT trained on one subsample of a given K_s^0 category is used to select events from the other subsample, in order to avoid bias. The input variables for the BDTs are the p_T , η , χ_{IP}^2 , χ_{VS}^2 , pointing angle and χ_{vtx}^2 of the B candidate; the sum χ_{IP}^2 of the h^+ and h^- ; the χ_{IP}^2 , χ_{VS}^2 and χ_{vtx}^2 of the K_s^0 candidate.

The selection requirement placed on the output of the BDTs is independently optimised for events containing K_s^0 candidates reconstructed in either Downstream or Long categories. Two different figures of merit are used to optimise the selection requirements, depending on whether the decay mode in question is favoured or suppressed. If favoured, the following is used

$$\mathcal{Q}_1 = \frac{S}{\sqrt{S+B}}, \quad (1)$$

where S (B) represents the number of expected signal (combinatorial background) events for a given selection. The value of S is estimated based on the known branching fractions and efficiencies, while B is calculated by fitting the sideband above the signal region and extrapolating into the signal region. If the mode is suppressed, an alternative figure of merit [32] is used

$$\mathcal{Q}_2 = \frac{\varepsilon_{\text{sig}}}{\frac{a}{2} + \sqrt{B}}, \quad (2)$$

where the signal efficiency (ε_{sig}) is estimated from the signal simulation. The value $a = 5$ is used in this analysis, which corresponds to optimising for 5σ significance to find the decay. This second figure of merit results in a more stringent requirement than the first. Hence, the requirements optimised with each figure of merit will from here on be referred to as the loose and tight BDT requirements, respectively.

The fraction of selected events containing more than one candidate is at the percent level. The candidate to be retained in each event is chosen arbitrarily.

A number of background contributions consisting of fully reconstructed B meson decays into two-body Dh or $c\bar{c}K_s^0$ combinations, result in a $K_s^0 h^+ h'^-$ final state and hence are, in terms of their B candidate invariant mass distribution, indistinguishable from signal candidates. The decays of Λ_b^0 baryons to $\Lambda_c^+ h$ with $\Lambda_c^+ \rightarrow p K_s^0$ also peak under the signal when the proton is misidentified. Therefore, the following D , Λ_c^+ and charmonia decays are explicitly reconstructed under the relevant particle hypotheses and vetoed in all the spectra: $D^0 \rightarrow K^- \pi^+$, $D^0 \rightarrow \pi^+ \pi^-$, $D^0 \rightarrow K^+ K^-$, $D^+ \rightarrow K_s^0 K^+$, $D^+ \rightarrow K_s^0 \pi^+$, $D_s^+ \rightarrow K_s^0 K^+$, $D_s^+ \rightarrow K_s^0 \pi^+$, and $\Lambda_c^+ \rightarrow p K_s^0$. Additional vetoes on charmonium resonances, $J/\psi \rightarrow \pi^+ \pi^-$, $\mu^+ \mu^-$, $K^+ K^-$ and $\chi_{c0} \rightarrow \pi^+ \pi^-$, $\mu^+ \mu^-$, $K^+ K^-$, are applied to remove the handful of fully reconstructed and well identified peaking $B_{(s)}^0 \rightarrow (J/\psi, \chi_{c0}) K_s^0$ decays. The veto for each reconstructed charm (charmonium) state R , $|m - m_R| < 30$ (48) MeV/c^2 , is defined around the world average mass value m_R [29] and the range is chosen according to the typical mass resolution obtained at LHCb.

Particle identification (PID) requirements are applied in addition to the selection described so far. The charged pion tracks from the K_s^0 decay and the charged tracks from the B decay are all required to be inconsistent with the muon track hypothesis. The logarithm of the likelihood ratio between the kaon and pion hypotheses ($DLL_{K\pi}$), mostly based on information from the RICH detectors [26], is used to discriminate between pion and kaon candidates from the B decay. Pion (kaon) candidates are required to satisfy $DLL_{K\pi} < 0$ ($DLL_{K\pi} > 5$). These are also required to be inconsistent with the proton hypothesis, in order to remove the possible contributions from charmless b -baryon decays. Pion (kaon) candidates are required to satisfy $DLL_{p\pi} < 10$ ($DLL_{pK} < 10$).

4 Fit model

A simultaneous unbinned extended maximum likelihood fit to the B -candidate invariant mass distributions of all decay channels is performed for each of the two BDT optimisations. In each simultaneous fit four types of components contribute, namely signal decays, cross-feed backgrounds, partially-reconstructed backgrounds, and combinatorial background.

Contributions from $B_{(s)}^0 \rightarrow K_s^0 h^+ h'^-$ decays with correct identification of the final state particles are modelled with sums of two Crystal Ball (CB) functions [33] that share common values for the peak position and width but have independent power law tails on opposite sides of the peak. The B^0 and B_s^0 masses (peak positions of the double-CB functions) are free in the fit. Four parameters related to the widths of the double-CB function are also free parameters of the fit: the common width of the $B^0 \rightarrow K_s^0 \pi^+ \pi^-$ and $B_s^0 \rightarrow K_s^0 \pi^+ \pi^-$ signals; the relative widths of $K_s^0 K^\pm \pi^\mp$ and $K_s^0 K^+ K^-$ to $K_s^0 \pi^+ \pi^-$, which are the same for B^0 and B_s^0 decay modes; the ratio of Long over Downstream widths, which is the same for all decay modes. These assumptions are made necessary by the otherwise poor determination of the width of the suppressed mode of each spectrum. The other parameters of the CB components are obtained by a simultaneous fit to simulated samples, constraining the fraction of events in the two CB components and the ratio of their tail parameters to be the same for all double-CB contributions.

Each selected candidate belongs uniquely to one reconstructed final state, by definition of the particle identification criteria. However, misidentified decays yield some cross-feed in the samples and are modelled empirically by single CB functions using simulated events. Only contributions from the decays $B^0 \rightarrow K_s^0 \pi^+ \pi^-$ and $B^0 \rightarrow K_s^0 K^+ K^-$ reconstructed and selected as $K_s^0 K^\pm \pi^\mp$, or the decays $B_s^0 \rightarrow K_s^0 K^\pm \pi^\mp$ and $B^0 \rightarrow K_s^0 K^\pm \pi^\mp$ reconstructed and selected as either $K_s^0 K^+ K^-$ or $K_s^0 \pi^+ \pi^-$ are considered. Other potential contributions are neglected. The relative yield of each misidentified decay is constrained with respect to the yield of the corresponding correctly identified decay. The constraints are implemented using Gaussian priors included in the likelihood. The mean values are obtained from the ratio of selection efficiencies and the resolutions include uncertainties originating from the finite size of the simulated events samples and the systematic uncertainties related to the determination of the PID efficiencies.

Partially reconstructed charmed transitions such as $B^- \rightarrow D^0 \pi^- (K^-)$ followed by

$D^0 \rightarrow K_s^0 \pi^+ \pi^-$, with a pion not reconstructed, are expected to dominate the background contribution in the lower invariant mass region. Charmless backgrounds such as from $B^0 \rightarrow \eta'(\rightarrow \rho^0 \gamma) K_s^0$, $B_s^0 \rightarrow K^{*0}(\rightarrow K_s^0 \pi^0) \bar{K}^{*0}(\rightarrow K^- \pi^+)$ and $B^+ \rightarrow K_s^0 \pi^+ \pi^- \pi^+$ decays are also expected to contribute with lower rates. These decays are modelled by means of generalised ARGUS functions [34] convolved with a Gaussian resolution function. Their parameters are determined from simulated samples. In order to reduce the number of components in the fit, only generic contributions for hadronic charmed and charmless decays are considered in each final state, however B^0 and B_s^0 contributions are explicitly included. Radiative decays and those from $B^0 \rightarrow \eta'(\rightarrow \rho^0 \gamma) K_s^0$ are considered separately and included only in the $K_s^0 \pi^+ \pi^-$ final state. The normalisation of all such contributions is constrained with Gaussian priors using the ratio of efficiencies from the simulation and the ratio of branching fractions from world averages [29]. Relative uncertainties on these ratios of 100%, 20% and 10% are considered for charmless, charmed, and radiative and $B^0 \rightarrow \eta'(\rightarrow \rho^0 \gamma) K_s^0$ decays, respectively.

The combinatorial background is modelled by an exponential function, where the slope parameter is fitted for each of the two K_s^0 reconstruction categories. The combinatorial backgrounds to the three final states $B_{(s)}^0 \rightarrow K_s^0 \pi^+ \pi^-$, $B_{(s)}^0 \rightarrow K_s^0 K^\pm \pi^\mp$ and $B_{(s)}^0 \rightarrow K_s^0 K^+ K^-$ are assumed to have identical slopes. This assumption as well as the choice of the exponential model are sources of systematic uncertainties.

The fit results for the two BDT optimisations are displayed in Figs. 1 and 2. Table 1 summarises the fitted yields of each decay mode for the optimisation used to determine the branching fractions. In the tight BDT optimisation the combinatorial background is negligible in the high invariant-mass region for the $K_s^0 \pi^+ \pi^-$ and $K_s^0 K^+ K^-$ final states, leading to a small systematic uncertainty related to the assumptions used to fit this component. An unambiguous first observation of $B_s^0 \rightarrow K_s^0 K^\pm \pi^\mp$ decays and a clear confirmation of the BaBar observation [17] of $B^0 \rightarrow K_s^0 K^\pm \pi^\mp$ decays are obtained. Significant yields for the $B_s^0 \rightarrow K_s^0 \pi^+ \pi^-$ decays are observed above negligible background with the tight optimisation of the selection. The likelihood profiles are shown in Fig. 3 for Downstream and Long K_s^0 samples separately. The $B_s^0 \rightarrow K_s^0 \pi^+ \pi^-$ decays are observed with a combined statistical significance of 6.2σ , which becomes 5.9σ including fit model systematic uncertainties. The statistical significance of the $B_s^0 \rightarrow K_s^0 K^+ K^-$ signal is at the level of 2.1σ combining Downstream and Long K_s^0 reconstruction categories.

5 Determination of the efficiencies

The measurements of the branching fractions of the $B_{(s)}^0 \rightarrow K_s^0 h^+ h'^-$ decays relative to the well established $B^0 \rightarrow K_s^0 \pi^+ \pi^-$ decay mode proceed according to

$$\frac{\mathcal{B}(B_{(s)}^0 \rightarrow K_s^0 h^+ h'^-)}{\mathcal{B}(B^0 \rightarrow K_s^0 \pi^+ \pi^-)} = \frac{\varepsilon_{B^0 \rightarrow K_s^0 \pi^+ \pi^-}^{\text{sel}}}{\varepsilon_{B_{(s)}^0 \rightarrow K_s^0 h^+ h'^-}^{\text{sel}}} \frac{N_{B_{(s)}^0 \rightarrow K_s^0 h^+ h'^-}}{N_{B^0 \rightarrow K_s^0 \pi^+ \pi^-}} \frac{f_d}{f_{d,s}}, \quad (3)$$

where ε^{sel} is the selection efficiency (which includes acceptance, reconstruction, selection, trigger and particle identification components), N is the fitted signal yield, and f_d and f_s

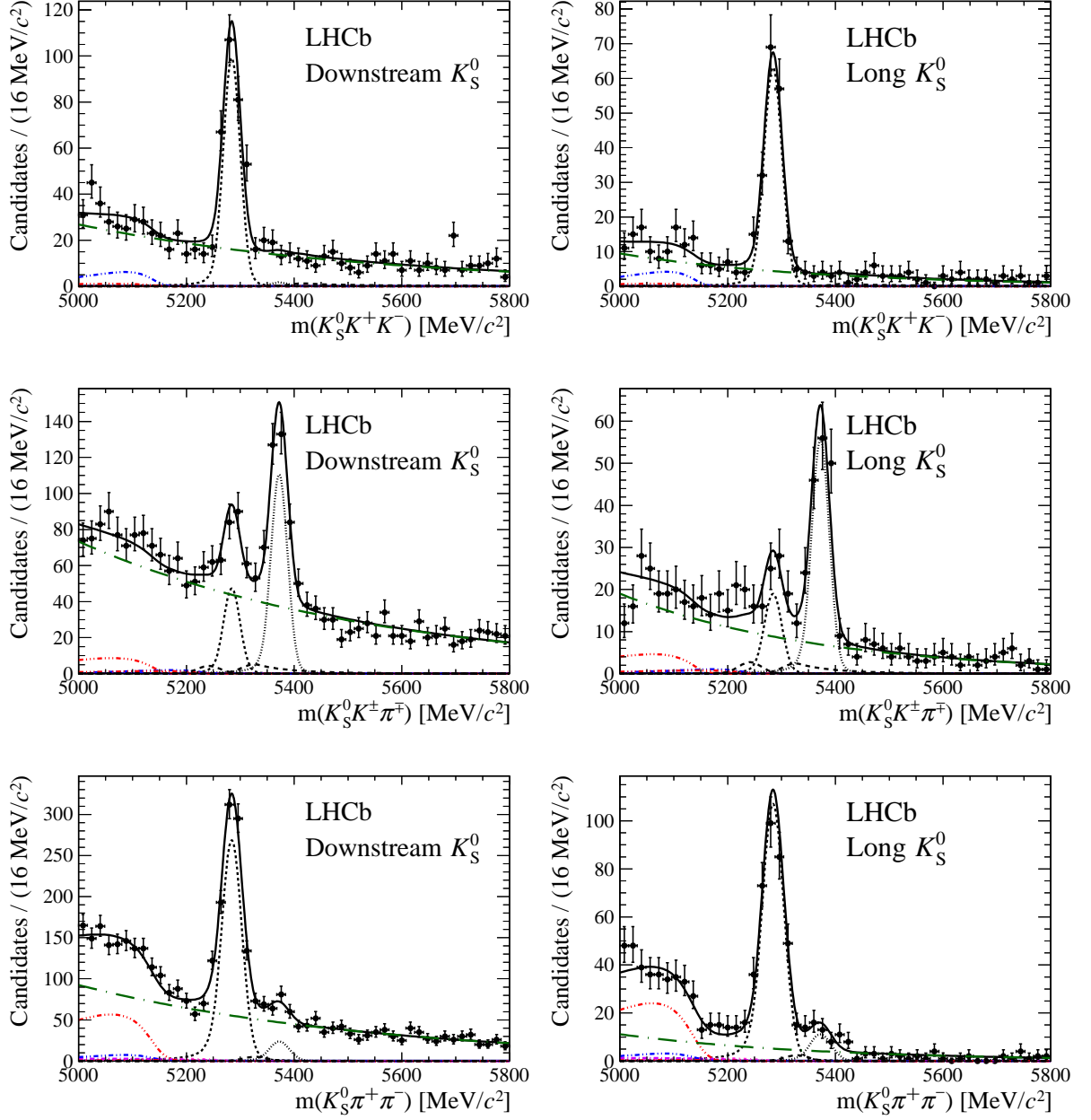


Figure 1: Invariant mass distributions of (top) $K_S^0 K^+ K^-$, (middle) $K_S^0 K^\pm \pi^\mp$, and (bottom) $K_S^0 \pi^+ \pi^-$ candidate events, with the loose selection for (left) Downstream and (right) Long K_S^0 reconstruction categories. In each plot, data are the black points with error bars and the total fit model is overlaid (solid black line). The B^0 (B_s^0) signal components are the black short-dashed (dotted) lines, while fully reconstructed misidentified decays are the black dashed lines close to the B^0 and B_s^0 peaks. The partially reconstructed contributions from B to open charm decays, charmless hadronic decays, $B^0 \rightarrow \eta'(\rightarrow \rho^0 \gamma) K_S^0$ and charmless radiative decays are the red dash triple-dotted, the blue dash double-dotted, the violet dash single-dotted, and the pink short-dash single-dotted lines, respectively. The combinatorial background contribution is the green long-dash dotted line.

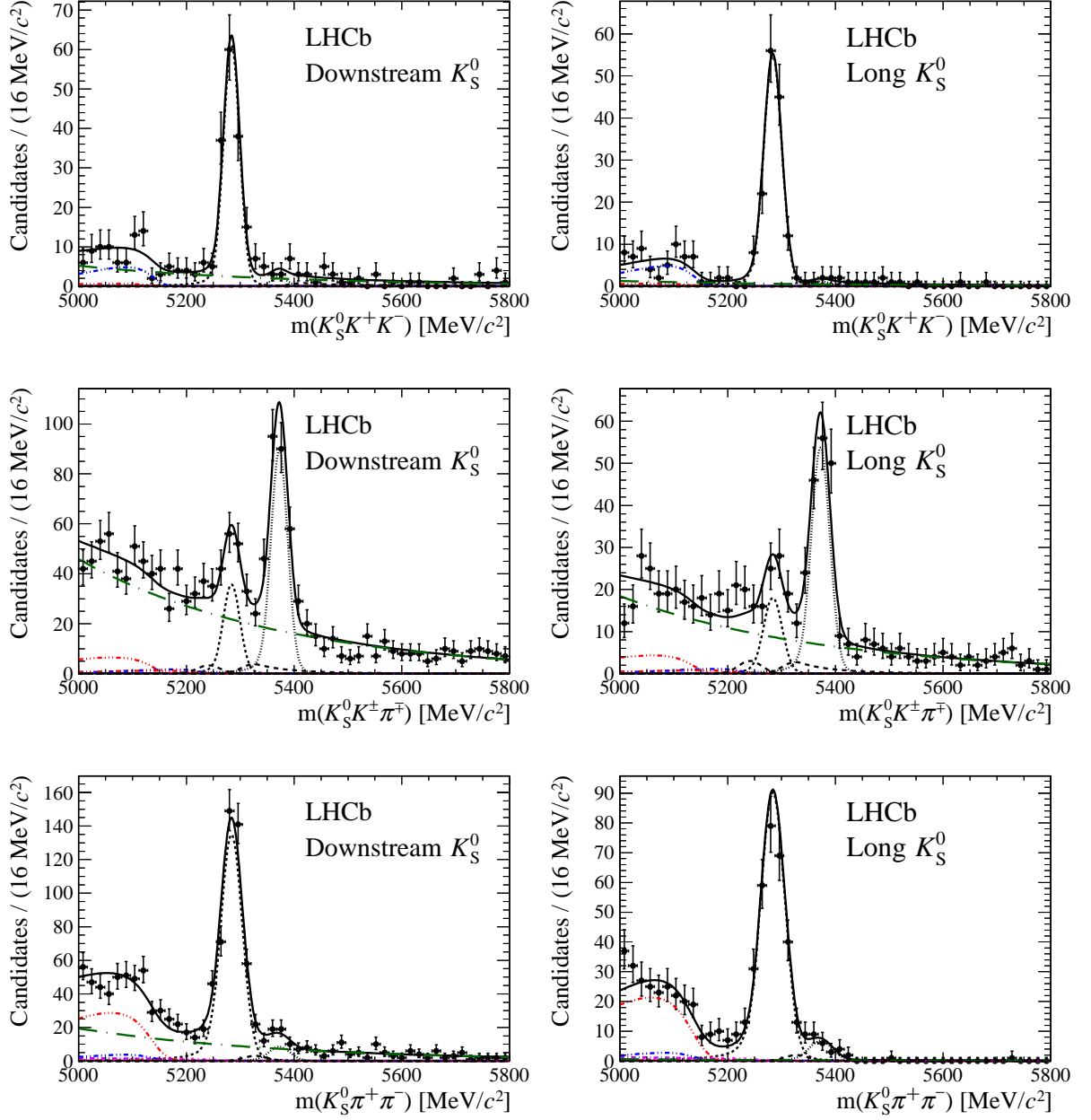


Figure 2: Invariant mass distributions of (top) $K_S^0 K^+ K^-$, (middle) $K_S^0 K^\pm \pi^\mp$, and (bottom) $K_S^0 \pi^+ \pi^-$ candidate events, with the tight selection for (left) Downstream and (right) Long K_S^0 reconstruction categories. In each plot, data are the black points with error bars and the total fit model is overlaid (solid black line). The B^0 (B_s^0) signal components are the black short-dashed (dotted) lines, while fully reconstructed misidentified decays are the black dashed lines close to the B^0 and B_s^0 peaks. The partially reconstructed contributions from B to open charm decays, charmless hadronic decays, $B^0 \rightarrow \eta'(\rightarrow \rho^0 \gamma) K_S^0$ and charmless radiative decays are the red dash triple-dotted, the blue dash double-dotted, the violet dash single-dotted, and the pink short-dash single-dotted lines, respectively. The combinatorial background contribution is the green long-dash dotted line.

Table 1: Yields obtained from the simultaneous fit corresponding to the chosen optimisation of the selection for each mode, where the uncertainties are statistical only. The average selection efficiencies are also given for each decay mode, where the uncertainties are due to the limited simulation sample size.

Mode	BDT	Downstream		Long	
		Yield	Efficiency (%)	Yield	Efficiency (%)
$B^0 \rightarrow K_s^0 \pi^+ \pi^-$	Loose	845 ± 38	0.0336 ± 0.0010	360 ± 21	0.0117 ± 0.0009
$B^0 \rightarrow K_s^0 K^+ K^-$	Loose	256 ± 20	0.0278 ± 0.0008	175 ± 15	0.0092 ± 0.0016
$B_s^0 \rightarrow K_s^0 K^\pm \pi^\mp$	Loose	283 ± 24	0.0316 ± 0.0007	152 ± 15	0.0103 ± 0.0008
$B^0 \rightarrow K_s^0 K^\pm \pi^\mp$	Tight	92 ± 15	0.0283 ± 0.0009	52 ± 11	0.0133 ± 0.0005
$B_s^0 \rightarrow K_s^0 \pi^+ \pi^-$	Tight	28 ± 9	0.0153 ± 0.0013	25 ± 6	0.0109 ± 0.0006
$B_s^0 \rightarrow K_s^0 K^+ K^-$	Tight	6 ± 4	0.0150 ± 0.0021	3 ± 3	0.0076 ± 0.0016

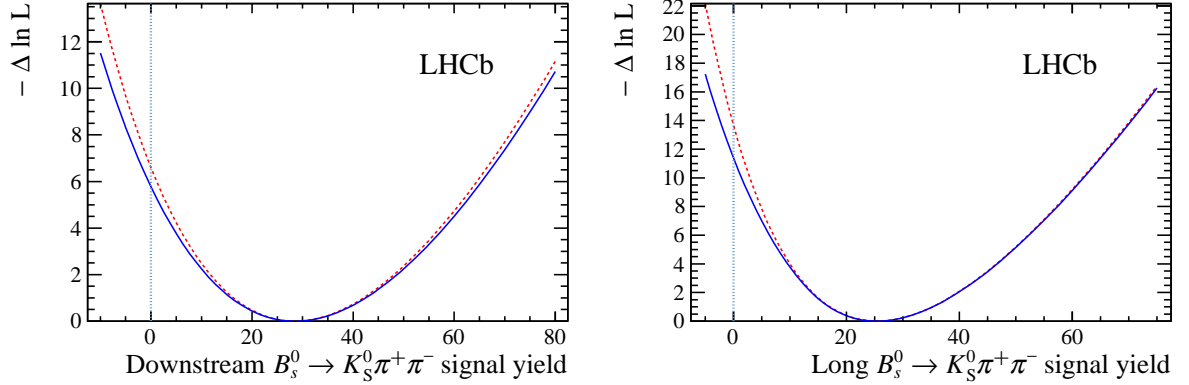


Figure 3: Likelihood profiles of the $B_s^0 \rightarrow K_s^0 \pi^+ \pi^-$ signal yield for the (left) Downstream and (right) Long K_s^0 samples. The dashed red line is the statistical-only profile, while the solid blue line also includes the fit model systematic uncertainties. The significance of the Downstream and Long signals are 3.4σ and 4.8σ , respectively, including systematic uncertainties. Combining Downstream and Long K_s^0 samples, an observation with 5.9σ , including systematic uncertainties, is obtained.

are the hadronisation fractions of a b quark into a B^0 and B_s^0 meson, respectively. The ratio f_s/f_d has been accurately determined by the LHCb experiment from hadronic and semileptonic measurements $f_s/f_d = 0.256 \pm 0.020$ [35].

Three-body decays are composed of several quasi-two-body decays and non-resonant contributions, all of them possibly interfering. Hence, their dynamical structure, described by the Dalitz plot [36], must be accounted for to correct for non-flat efficiencies over the phase space. Since the dynamics of most of the modes under study are not known prior to this analysis, efficiencies are determined for each decay mode from simulated signal samples

in bins of the “square Dalitz plot” [37], where the usual Dalitz-plot coordinates have been transformed into a rectangular space. The edges of the usual Dalitz plot are spread out in the square Dalitz plot, which permits a more precise modelling of the efficiency variations in the regions where they are most strongly varying and where most of the signal events are expected. Two complementary simulated samples have been produced, corresponding to events generated uniformly in phase space or uniformly in the square Dalitz plot. The square Dalitz-plot distribution of each signal mode is determined from the data using the *sPlot* technique [38]. The binning is chosen such that each bin is populated by approximately the same number of signal events. The average efficiency for each decay mode is calculated as the weighted harmonic mean over the bins. The average weighted selection efficiencies are summarised in Table 1 and depend on the final state, the K_s^0 reconstruction category, and the choice of the BDT optimisation. Their relative uncertainties due to the finite size of the simulated event samples vary from 3% to 17%, reflecting the different dynamical structures of the decay modes.

The particle identification and misidentification efficiencies are determined from simulated signal events on an event-by-event basis by adjusting the DLL distributions measured from calibration events to match the kinematical properties of the tracks in the decay of interest. The reweighting is performed in bins of p and p_T , accounting for kinematic correlations between the tracks. Calibration tracks are taken from $D^{*+} \rightarrow D^0 \pi_s^+$ decays where the D^0 decays to the Cabibbo-favoured $K^- \pi^+$ final state. The charge of the soft pion π_s^+ hence provides the kaon or pion identity of the tracks. The dependence of the PID efficiency over the Dalitz plot is included in the procedure described above. This calibration is performed using samples from the same data taking period, accounting for the variation in the performance of the RICH detectors over time.

6 Systematic uncertainties

Most of the systematic uncertainties are eliminated or greatly reduced by normalising the branching fraction measurements with respect to the $B^0 \rightarrow K_s^0 \pi^+ \pi^-$ mode. The remaining sources of systematic effects and the methods used to estimate the corresponding uncertainties are described in this section. In addition to the systematic effects related to the measurements performed in this analysis, there is that associated with the measured value of f_s/f_d . A summary of the contributions, expressed as relative uncertainties, is given in Table 2.

6.1 Fit model

The fit model relies on a number of assumptions, both in the values of parameters being taken from simulation and in the choice of the functional forms describing the various contributions.

The uncertainties linked to the parameters fixed to values determined from simulated events are obtained by repeating the fit while the fixed parameters are varied according to

their uncertainties using pseudo-experiments. For example, the five fixed parameters of the CB functions describing the signals, as well as the ratio of resolutions with respect to $B^0 \rightarrow K_s^0 \pi^+ \pi^-$ decays, are varied according to their correlation matrix determined from simulated events. The nominal fit is then performed on this sample of pseudo-experiments and the distribution of the difference between the yield determined in each of these fits and that of the nominal fit is fitted with a Gaussian function. The systematic uncertainty associated with the choice of the value of each signal parameter from simulated events is then assigned as the linear sum of the absolute value of the mean of the Gaussian and its resolution. An identical procedure is employed to obtain the systematic uncertainties related to the fixed parameters of the ARGUS functions describing the partially reconstructed backgrounds and the CB functions used for the cross-feeds.

The uncertainties related to the choice of the models used in the nominal fit are evaluated for the signal and combinatorial background models only. Both the partially reconstructed background and the cross-feed shapes suffer from a large statistical uncertainty from the simulated event samples and therefore the uncertainty related to the fixed parameters also covers any sensible variation of the shape. The B_s^0 decay modes that are studied lie near large B^0 contributions for the $K_s^0 \pi^+ \pi^-$ and $K_s^0 K^+ K^-$ spectra. The impact of the modelling of the right hand side of the B^0 mass distribution is addressed by removing the second CB function, used as an alternative model.

For the combinatorial background, a unique slope parameter governs the shape of each K_s^0 reconstruction category (Long or Downstream). Two alternative models are considered: allowing independent slopes for each of the six spectra (testing the assumption of a universal slope) and using a linear model in place of the exponential (testing the functional form of the combinatorial shape). Pseudo-experiments are again used to estimate the effect of these alternative models; in the former case, the value and uncertainties to be considered for the six slopes are determined from a fit to the data. The dataset is generated according to the substitute model and the fit is performed to the generated sample using the nominal model. The value of the uncertainty is again estimated as the linear sum of the absolute value of the resulting bias and its resolution. The total fit model systematic uncertainty is given by the sum in quadrature of all the contributions and is mostly dominated by the combinatorial background model uncertainty.

6.2 Selection and trigger efficiencies

The accuracy of the efficiency determination is limited in most cases by the finite size of the samples of simulated signal events, duly propagated as a systematic uncertainty. In addition, the effect related to the choice of binning for the square Dalitz plot is estimated from the spread of the average efficiencies determined from several alternative binning schemes. Good agreement between data and the simulation is obtained, hence no further systematic uncertainty is assigned.

Systematic uncertainties related to the hardware stage trigger have been studied. A data control sample of $D^{*+} \rightarrow D^0(\rightarrow K^- \pi^+) \pi_s^+$ decays is used to quantify differences between pions and kaons, separated by positive and negative hadron charges, as a function

Table 2: Systematic uncertainties on the ratio of branching fractions for Downstream and Long K_s^0 reconstruction. All uncertainties are relative and are quoted as percentages.

Downstream	Fit	Selection	Trigger	PID	Total	f_s/f_d
$\mathcal{B}(B^0 \rightarrow K_s^0 K^\pm \pi^\mp) / \mathcal{B}(B^0 \rightarrow K_s^0 \pi^+ \pi^-)$	5	6	3	1	8	—
$\mathcal{B}(B^0 \rightarrow K_s^0 K^+ K^-) / \mathcal{B}(B^0 \rightarrow K_s^0 \pi^+ \pi^-)$	1	5	3	1	6	—
$\mathcal{B}(B_s^0 \rightarrow K_s^0 \pi^+ \pi^-) / \mathcal{B}(B^0 \rightarrow K_s^0 \pi^+ \pi^-)$	8	16	2	1	18	8
$\mathcal{B}(B_s^0 \rightarrow K_s^0 K^\pm \pi^\mp) / \mathcal{B}(B^0 \rightarrow K_s^0 \pi^+ \pi^-)$	2	5	1	1	6	8
$\mathcal{B}(B_s^0 \rightarrow K_s^0 K^+ K^-) / \mathcal{B}(B^0 \rightarrow K_s^0 \pi^+ \pi^-)$	1	18	3	1	18	8
Long						
$\mathcal{B}(B^0 \rightarrow K_s^0 K^\pm \pi^\mp) / \mathcal{B}(B^0 \rightarrow K_s^0 \pi^+ \pi^-)$	5	10	1	1	14	—
$\mathcal{B}(B^0 \rightarrow K_s^0 K^+ K^-) / \mathcal{B}(B^0 \rightarrow K_s^0 \pi^+ \pi^-)$	3	20	1	1	20	—
$\mathcal{B}(B_s^0 \rightarrow K_s^0 \pi^+ \pi^-) / \mathcal{B}(B^0 \rightarrow K_s^0 \pi^+ \pi^-)$	5	10	1	1	11	8
$\mathcal{B}(B_s^0 \rightarrow K_s^0 K^\pm \pi^\mp) / \mathcal{B}(B^0 \rightarrow K_s^0 \pi^+ \pi^-)$	3	12	2	1	13	8
$\mathcal{B}(B_s^0 \rightarrow K_s^0 K^+ K^-) / \mathcal{B}(B^0 \rightarrow K_s^0 \pi^+ \pi^-)$	2	22	1	1	22	8

of p_T [27]. Though they show an overall good agreement for the different types of tracks, the efficiency for pions is slightly smaller than for kaons at high p_T . Simulated events are reweighted by these data-driven calibration curves in order to extract the hadron trigger efficiency for each mode, propagating properly the calibration-related uncertainties. Finally, the ageing of the calorimeters during the data taking period when the data sample analysed was recorded induced changes in the absolute scale of the trigger efficiencies. While this was mostly mitigated by periodic recalibration, relative variations occurred of order 10%. Since the kinematics vary marginally from one mode to the other, a systematic effect on the ratio of efficiencies arises. It is fully absorbed by increasing the trigger efficiency systematic uncertainty by 10%.

6.3 Particle identification efficiencies

The procedure to evaluate the efficiencies of the PID selections uses calibration tracks that differ from the signal tracks in terms of their kinematic distributions. While the binning procedure attempts to mitigate these differences there could be some remaining systematic effect. To quantify any bias due to the procedure, simulated samples of the control modes are used in place of the data samples. The average efficiency determined from these samples can then be compared with the efficiency determined from simply applying the selections to the simulated signal samples. The differences are found to be less than 1%, hence no correction is applied. The calibration procedure is assigned a systematic uncertainty. The observed differences in efficiencies are multiplied by the efficiency ratio and statistical uncertainties from the finite sample sizes are added in quadrature.

7 Results and conclusion

The 2011 LHCb dataset, corresponding to an integrated luminosity of 1.0 fb^{-1} recorded at a centre-of-mass energy of 7 TeV, has been analysed to search for the decays $B_{(s)}^0 \rightarrow K_s^0 h^+ h'^-$. The decays $B_s^0 \rightarrow K_s^0 K^\pm \pi^\mp$ and $B_s^0 \rightarrow K_s^0 \pi^+ \pi^-$ are observed for the first time. The former is unambiguous, while for the latter the significance of the observation is 5.9 standard deviations, including statistical and systematic uncertainties. The decay mode $B^0 \rightarrow K_s^0 K^\pm \pi^\mp$, previously observed by the BaBar experiment [17], is confirmed. The efficiency-corrected Dalitz-plot distributions of the three decay modes $B_s^0 \rightarrow K_s^0 \pi^+ \pi^-$, $B_s^0 \rightarrow K_s^0 K^\pm \pi^\mp$, and $B^0 \rightarrow K_s^0 K^\pm \pi^\mp$ are displayed in Fig. 4. Some structure is evident at low $K_s^0 \pi^\pm$ and $K^\pm \pi^\mp$ invariant masses in the $B_s^0 \rightarrow K_s^0 K^\pm \pi^\mp$ decay mode, while in the $B^0 \rightarrow K_s^0 K^\pm \pi^\mp$ decay the largest structure is seen in the low $K_s^0 K^\pm$ invariant mass region. No significant evidence for $B_s^0 \rightarrow K_s^0 K^+ K^-$ decays is obtained. A 90% confidence level (CL) interval based on the CL inferences described in Ref. [39] is hence placed on the branching fraction for this decay mode.

Each branching fraction is measured (or limited) relative to that of $B^0 \rightarrow K_s^0 \pi^+ \pi^-$. The ratios of branching fractions are determined independently for the two K_s^0 reconstruction categories and then combined by performing a weighted average, excluding the uncertainty due to the ratio of hadronisation fractions, since it is fully correlated between the two categories. The Downstream and Long results all agree within two standard deviations, including statistical and systematic uncertainties. The results obtained from the combination are

$$\begin{aligned}
 \frac{\mathcal{B}(B^0 \rightarrow K_s^0 K^\pm \pi^\mp)}{\mathcal{B}(B^0 \rightarrow K_s^0 \pi^+ \pi^-)} &= 0.128 \pm 0.017 \text{ (stat.)} \pm 0.009 \text{ (syst.)}, \\
 \frac{\mathcal{B}(B^0 \rightarrow K_s^0 K^+ K^-)}{\mathcal{B}(B^0 \rightarrow K_s^0 \pi^+ \pi^-)} &= 0.385 \pm 0.031 \text{ (stat.)} \pm 0.023 \text{ (syst.)}, \\
 \frac{\mathcal{B}(B_s^0 \rightarrow K_s^0 \pi^+ \pi^-)}{\mathcal{B}(B^0 \rightarrow K_s^0 \pi^+ \pi^-)} &= 0.29 \pm 0.06 \text{ (stat.)} \pm 0.03 \text{ (syst.)} \pm 0.02 \text{ (} f_s/f_d \text{)}, \\
 \frac{\mathcal{B}(B_s^0 \rightarrow K_s^0 K^\pm \pi^\mp)}{\mathcal{B}(B^0 \rightarrow K_s^0 \pi^+ \pi^-)} &= 1.48 \pm 0.12 \text{ (stat.)} \pm 0.08 \text{ (syst.)} \pm 0.12 \text{ (} f_s/f_d \text{)}, \\
 \frac{\mathcal{B}(B_s^0 \rightarrow K_s^0 K^+ K^-)}{\mathcal{B}(B^0 \rightarrow K_s^0 \pi^+ \pi^-)} &\in [0.004; 0.068] \text{ at } 90\% \text{ CL}.
 \end{aligned}$$

The measurement of the relative branching fractions of $B^0 \rightarrow K_s^0 K^\pm \pi^\mp$ and $B^0 \rightarrow K_s^0 K^+ K^-$ are in good agreement with, and slightly more precise than, the previous world average results [8, 10, 11, 17, 29, 40, 41]. Using the world average value, $\mathcal{B}(B^0 \rightarrow K^0 \pi^+ \pi^-) =$

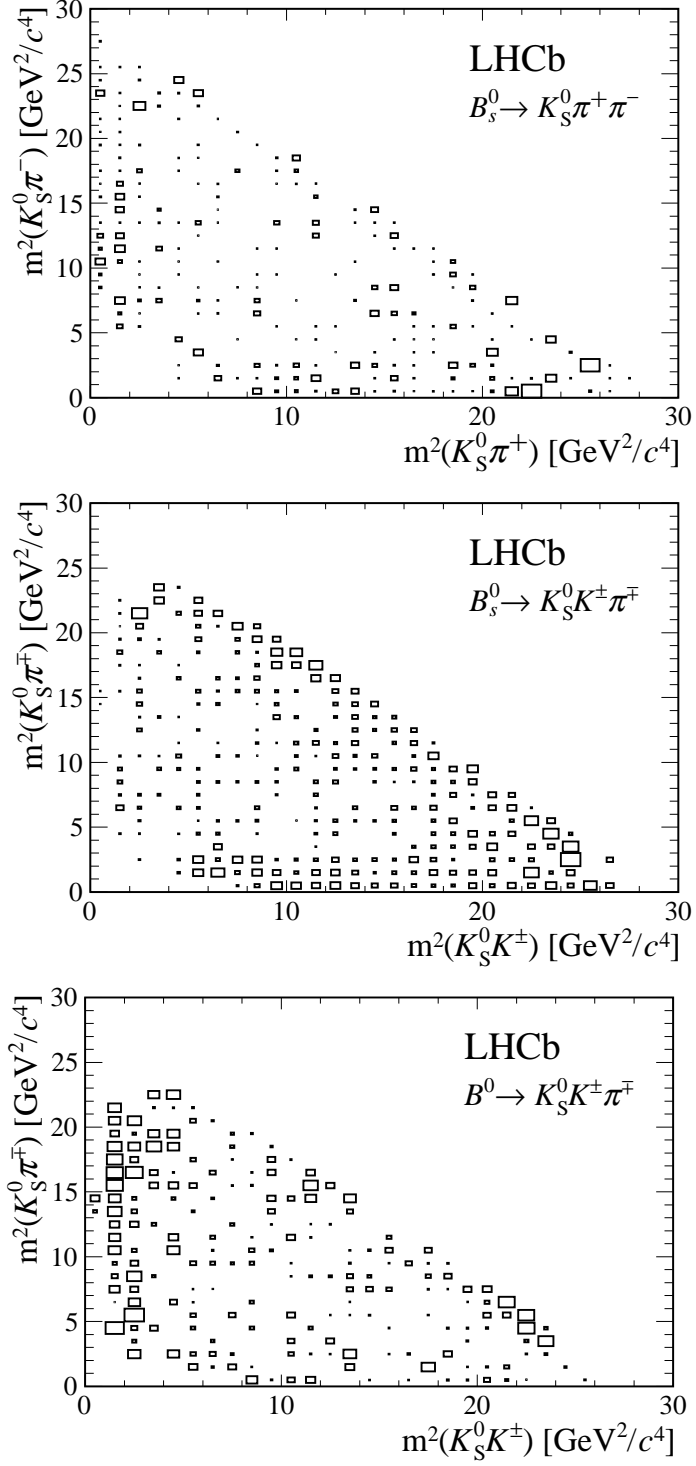


Figure 4: Efficiency-corrected Dalitz-plot distributions, produced using the *sPlot* procedure, of (top) $B_s^0 \rightarrow K_S^0 \pi^+ \pi^-$, (middle) $B_s^0 \rightarrow K_S^0 K^\pm \pi^\mp$ and (bottom) $B^0 \rightarrow K_S^0 K^\pm \pi^\mp$ events. Bins with negative content appear empty.

$(4.96 \pm 0.20) \times 10^{-5}$ [11, 29], the measured time-integrated branching fractions

$$\begin{aligned}
\mathcal{B}(B^0 \rightarrow K^0 K^\pm \pi^\mp) &= (6.4 \pm 0.9 \pm 0.4 \pm 0.3) \times 10^{-6}, \\
\mathcal{B}(B^0 \rightarrow K^0 K^+ K^-) &= (19.1 \pm 1.5 \pm 1.1 \pm 0.8) \times 10^{-6}, \\
\mathcal{B}(B_s^0 \rightarrow K^0 \pi^+ \pi^-) &= (14.3 \pm 2.8 \pm 1.8 \pm 0.6) \times 10^{-6}, \\
\mathcal{B}(B_s^0 \rightarrow K^0 K^\pm \pi^\mp) &= (73.6 \pm 5.7 \pm 6.9 \pm 3.0) \times 10^{-6}, \\
\mathcal{B}(B_s^0 \rightarrow K^0 K^+ K^-) &\in [0.2; 3.4] \times 10^{-6} \text{ at } 90\% \text{ CL},
\end{aligned}$$

are obtained, where the first uncertainty is statistical, the second systematic and the last due to the uncertainty on $\mathcal{B}(B^0 \rightarrow K^0 \pi^+ \pi^-)$.

The first observation of the decay modes $B_s^0 \rightarrow K_s^0 \pi^+ \pi^-$ and $B_s^0 \rightarrow K_s^0 K^\pm \pi^\mp$ is an important step towards extracting information on the mixing-induced CP -violating phase in the B_s^0 system and the weak phase γ from these decays. The apparent rich structure of the Dalitz plots, particularly for the $B_{(s)}^0 \rightarrow K_s^0 K^\pm \pi^\mp$ decays, motivates future amplitude analyses of these $B_{(s)}^0 \rightarrow K_s^0 h^+ h'^-$ modes with larger data samples.

Acknowledgements

We express our gratitude to our colleagues in the CERN accelerator departments for the excellent performance of the LHC. We thank the technical and administrative staff at the LHCb institutes. We acknowledge support from CERN and from the national agencies: CAPES, CNPq, FAPERJ and FINEP (Brazil); NSFC (China); CNRS/IN2P3 and Region Auvergne (France); BMBF, DFG, HGF and MPG (Germany); SFI (Ireland); INFN (Italy); FOM and NWO (The Netherlands); SCSR (Poland); MEN/IFA (Romania); MinES, Rosatom, RFBR and NRC ‘‘Kurchatov Institute’’ (Russia); MinECo, XuntaGal and GENCAT (Spain); SNSF and SER (Switzerland); NAS Ukraine (Ukraine); STFC (United Kingdom); NSF (USA). We also acknowledge the support received from the ERC under FP7. The Tier1 computing centres are supported by IN2P3 (France), KIT and BMBF (Germany), INFN (Italy), NWO and SURF (The Netherlands), PIC (Spain), GridPP (United Kingdom). We are thankful for the computing resources put at our disposal by Yandex LLC (Russia), as well as to the communities behind the multiple open source software packages that we depend on.

References

- [1] N. Cabibbo, *Unitary symmetry and leptonic decays*, Phys. Rev. Lett. **10** (1963) 531.
- [2] M. Kobayashi and T. Maskawa, *CP violation in the renormalizable theory of weak interaction*, Prog. Theor. Phys. **49** (1973) 652.
- [3] G. Buchalla, G. Hiller, Y. Nir, and G. Raz, *The pattern of CP asymmetries in $b \rightarrow s$ transitions*, JHEP **09** (2005) 074, [arXiv:hep-ph/0503151](https://arxiv.org/abs/hep-ph/0503151).

- [4] Y. Grossman and M. P. Worah, *CP asymmetries in B decays with new physics in decay amplitudes*, Phys. Lett. **B395** (1997) 241, [arXiv:hep-ph/9612269](#).
- [5] D. London and A. Soni, *Measuring the CP angle β in hadronic $b \rightarrow s$ penguin decays*, Phys. Lett. **B407** (1997) 61, [arXiv:hep-ph/9704277](#).
- [6] M. Ciuchini *et al.*, *CP violating B decays in the Standard Model and Supersymmetry*, Phys. Rev. Lett. **79** (1997) 978, [arXiv:hep-ph/9704274](#).
- [7] Belle collaboration, J. Dalseno *et al.*, *Time-dependent Dalitz-plot measurement of CP parameters in $B^0 \rightarrow K_s^0 \pi^+ \pi^-$ decays*, Phys. Rev. **D79** (2009) 072004, [arXiv:0811.3665](#).
- [8] BaBar collaboration, B. Aubert *et al.*, *Time-dependent amplitude analysis of $B^0 \rightarrow K_s^0 \pi^+ \pi^-$* , Phys. Rev. **D80** (2009) 112001, [arXiv:0905.3615](#).
- [9] Belle collaboration, Y. Nakahama *et al.*, *Measurement of CP violating asymmetries in $B^0 \rightarrow K_s^0 K^+ K^-$ decays with a time-dependent Dalitz approach*, Phys. Rev. **D82** (2010) 073011, [arXiv:1007.3848](#).
- [10] BaBar Collaboration, J. P. Lees *et al.*, *Study of CP violation in Dalitz-plot analyses of $B^0 \rightarrow K_s^0 K^+ K^-$, $B^+ \rightarrow K^+ K^- K^+$, and $B^+ \rightarrow K_s^0 K_s^0 K^+$* , Phys. Rev. **D85** (2012) 112010, [arXiv:1201.5897](#).
- [11] Heavy Flavor Averaging Group, Y. Amhis *et al.*, *Averages of b-hadron, c-hadron, and τ -lepton properties as of early 2012*, [arXiv:1207.1158](#), updated results and plots available at: <http://www.slac.stanford.edu/xorg/hfag/>.
- [12] L. Silvestrini, *Searching for new physics in $b \rightarrow s$ hadronic penguin decays*, Ann. Rev. Nucl. Part. Sci. **57** (2007) 405, [arXiv:0705.1624](#).
- [13] M. Ciuchini, M. Pierini, and L. Silvestrini, *New bounds on the CKM matrix from $B \rightarrow K \pi \pi$ Dalitz-plot analyses*, Phys. Rev. **D74** (2006) 051301, [arXiv:hep-ph/0601233](#).
- [14] M. Gronau, D. Pirjol, A. Soni, and J. Zupan, *Improved method for CKM constraints in charmless three-body B and B_s^0 decays*, Phys. Rev. **D75** (2007) 014002, [arXiv:hep-ph/0608243](#).
- [15] BaBar collaboration, J. P. Lees *et al.*, *Amplitude analysis of $B^0 \rightarrow K^+ \pi^- \pi^0$ and evidence of direct CP violation in $B \rightarrow K^* \pi$ decays*, Phys. Rev. **D83** (2011) 112010, [arXiv:1105.0125](#).
- [16] M. Ciuchini, M. Pierini, and L. Silvestrini, *Hunting the CKM weak phase with time-integrated Dalitz analyses of $B_s^0 \rightarrow K \pi \pi$ decays*, Phys. Lett. **B645** (2007) 201, [arXiv:hep-ph/0602207](#).
- [17] BaBar collaboration, P. del Amo Sanchez *et al.*, *Observation of the rare decay $B^0 \rightarrow K_s^0 K^\pm \pi^\mp$* , Phys. Rev. **D82** (2010) 031101, [arXiv:1003.0640](#).

- [18] K. De Bruyn *et al.*, *Branching ratio measurements of B_s^0 decays*, Phys. Rev. **D86** (2012) 014027, [arXiv:1204.1735](#).
- [19] T. Sjöstrand, S. Mrenna, and P. Skands, *PYTHIA 6.4 physics and manual*, JHEP **05** (2006) 026, [arXiv:hep-ph/0603175](#).
- [20] I. Belyaev *et al.*, *Handling of the generation of primary events in GAUSS, the LHCb simulation framework*, Nuclear Science Symposium Conference Record (NSS/MIC) **IEEE** (2010) 1155.
- [21] D. J. Lange, *The EvtGen particle decay simulation package*, Nucl. Instrum. Meth. **A462** (2001) 152.
- [22] P. Golonka and Z. Was, *PHOTOS Monte Carlo: a precision tool for QED corrections in Z and W decays*, Eur. Phys. J. **C45** (2006) 97, [arXiv:hep-ph/0506026](#).
- [23] Geant4 collaboration, J. Allison *et al.*, *Geant4 developments and applications*, IEEE Trans. Nucl. Sci. **53** (2006) 270; Geant4 collaboration, S. Agostinelli *et al.*, *Geant4: a simulation toolkit*, Nucl. Instrum. Meth. **A506** (2003) 250.
- [24] M. Clemencic *et al.*, *The LHCb simulation application, GAUSS: design, evolution and experience*, J. Phys.: Conf. Ser. **331** (2011) 032023.
- [25] LHCb collaboration, A. A. Alves Jr. *et al.*, *The LHCb detector at the LHC*, JINST **3** (2008) S08005.
- [26] M. Adinolfi *et al.*, *Performance of the LHCb RICH detector at the LHC*, Eur. Phys. J. **C73** (2013) 2431, [arXiv:1211.6759](#).
- [27] R. Aaij *et al.*, *The LHCb trigger and its performance in 2011*, JINST **8** (2013) P04022, [arXiv:1211.3055](#).
- [28] V. V. Gligorov and M. Williams, *Efficient, reliable and fast high-level triggering using a bonsai boosted decision tree*, JINST **8** (2013) P02013, [arXiv:1210.6861](#).
- [29] Particle Data Group, J. Beringer *et al.*, *Review of particle physics*, Phys. Rev. **D86** (2012) 010001.
- [30] L. Breiman, J. H. Friedman, R. A. Olshen, and C. J. Stone, *Classification and regression trees*, Wadsworth international group, Belmont, California, USA, 1984.
- [31] R. E. Schapire and Y. Freund, *A decision-theoretic generalization of on-line learning and an application to boosting*, Jour. Comp. and Syst. Sc. **55** (1997) 119.
- [32] G. Punzi, *Sensitivity of searches for new signals and its optimization*, eConf **C030908** (2003) MODT002, [arXiv:physics/0308063](#).

- [33] T. Skwarnicki, *A study of the radiative cascade transitions between the Upsilon-prime and Upsilon resonances*, PhD thesis, Institute of Nuclear Physics, Krakow, 1986, DESY-F31-86-02.
- [34] ARGUS collaboration, H. Albrecht *et al.*, *Exclusive hadronic decays of B mesons*, Z. Phys. **C48** (1990) 543.
- [35] LHCb collaboration, R. Aaij *et al.*, *Measurement of the fragmentation fraction ratio f_s/f_d and its dependence on B meson kinematics*, JHEP **04** (2013) 1, arXiv:1301.5286.
- [36] R. H. Dalitz, *On the analysis of tau-meson data and the nature of the tau-meson*, Phil. Mag. **44** (1953) 1068.
- [37] BaBar collaboration, B. Aubert *et al.*, *An amplitude analysis of the decay $B^\pm \rightarrow \pi^\pm \pi^\pm \pi^\mp$* , Phys. Rev. **D72** (2005) 052002, arXiv:hep-ex/0507025.
- [38] M. Pivk and F. R. Le Diberder, *sPlot: a statistical tool to unfold data distributions*, Nucl. Instrum. Meth. **A555** (2005) 356, arXiv:physics/0402083.
- [39] G. J. Feldman and R. D. Cousins, *A unified approach to the classical statistical analysis of small signals*, Phys. Rev. **D57** (1998) 3873.
- [40] Belle collaboration, A. Garmash *et al.*, *Study of B meson decays to three body charmless hadronic final states*, Phys. Rev. **D69** (2004) 012001, arXiv:hep-ex/0307082.
- [41] Belle Collaboration, A. Garmash *et al.*, *Dalitz analysis of three-body charmless $B^0 \rightarrow K^0 \pi^+ \pi^-$ decay*, Phys. Rev. **D75** (2007) 012006, arXiv:hep-ex/0610081.